

Electric field enhances the electronic and diffusion properties of penta-graphene nanoribbons for application in lithium-ion batteries: a first-principles study

Thi Nhan Tran¹, Nguyen Vo Anh Duy², Nguyen Hoang Hieu³, Truc Anh Nguyen⁴, Nguyen To Van⁵, Viet Bac Thi Phung^{6,7}, Peter Schall⁸, and Minh Triet Dang^{*3}

¹Faculty of Fundamental Sciences, Hanoi University of Industry, 298 Cau Dien Street, Bac Tu Liem, Hanoi 100000, Vietnam.

²FPT university, 600 Nguyen Van Cu, Ninh Kieu District, Can Tho, Vietnam.

³Can Tho University, 3/2 Street, Ninh Kieu District, Can Tho, Vietnam.

⁴Faculty of Mechanics, Can Tho University of Technology, 256 Nguyen Van Cu Street, Ninh Kieu, Can Tho, Vietnam

⁵Faculty of Chemico-Physical Engineering, Le Quy Don Technical University, Ha Noi 100000, Vietnam

⁶Center for Environmental Intelligence and College of Engineering & Computer Science, VinUniversity, Hanoi 100000, Vietnam.

⁷Institute of Sustainability Science, VNU Vietnam Japan University, Vietnam National University, Hanoi 100000, Vietnam

⁸Van der Waals-Zeeman Institute, University of Amsterdam, Science Park 904, Amsterdam, The Netherlands

* Email: dmtriet@ctu.edu.vn

Abstract. Enhancing the electronic and diffusion properties of lithium-ion batteries is crucial for improving the performance of the fast-growing energy storage devices. Here we use first principles methods with density functional theory and the climbing image-nudged elastic band method to evaluate the impact of an external electric field on the stability, electronic and diffusion properties of penta-graphene nanoribbons upon lithium adsorption. We show that by adsorbing a lithium atom, these semiconductor nanoribbons become metal with a formation energy of - 0.22 (eV). The diffusion coefficient of this material is five orders of magnitude higher than that of a common carbon graphite layer. Under a relatively small vertical electric field, these lithium-ion systems are even more stable, and their diffusion coefficient is enhanced significantly of ~711 times higher than that of the material in the absence of an applied electric field and ~520 times higher than in the case of commercial graphitic carbon layers. Our results highlight the role of an external electric field as a novel switch to improve the efficiency of lithium-ion batteries with penta-graphene nanoribbon electrodes and open a new horizon for the use of more environmentally friendly pentagonal materials as electrode materials in lithium-ion battery industry.

1. Introduction

Lithium-ion rechargeable battery industry is a fast-growing market for mobile devices and electric vehicles [1]. Due to the rapid demand of the society and the shortage of raw material supply, the cost of rechargeable lithium-ion batteries (LIBs) is currently very high and keeps increasing [2]. This drawback limits the applicability of these types of batteries both in industry and for societal needs. The urgent need is to reduce the cost for fabricating LIBs and to improve the electrochemical performance such as high reversible capacity, high conductivity, reasonable cycling life and environmentally friendly manufacturing. Typical LIBs consist of anode and cathode electrodes, a separator, and all immersed electrolyte solution. Several commercial types of cathode electrode materials for LIBs are LiCoO_2 (LCO) [3], [4], LiMnO_2 (LMO) [5], [6], LiFePO_4 (LPO) [7], [8], and $\text{Li}[\text{Ni}_x\text{Mn}_y\text{Co}_z]\text{O}_2$ (NMC) [9]. To fulfil the aforementioned requirements, two critical tasks are improving the performance of cathode and/or anode electrode materials. For high quality and large energy storage LIBs, nickel-rich NMC layered cathodes can be considered as an excellent candidate to reconcile the requirement of high specific discharge capacity, reasonable durability and working voltages, and affordable production cost [10]. NMC materials share almost the same specific energy density with LCO cathode materials but possess a better discharge rate and lower cost, while their durability is as high as that of LFO [11]. Some typical NMC materials are $\text{LiNi}_{1/3}\text{Mn}_{1/3}\text{Co}_{1/3}\text{O}_2$ (NMC111), $\text{LiNi}_{0.6}\text{Mn}_{0.2}\text{Co}_{0.2}\text{O}_2$ (NMC622) and $\text{LiNi}_{0.8}\text{Mn}_{0.1}\text{Co}_{0.1}\text{O}_2$ (NMC811). Recently, we proposed a modified co-precipitation method to synthesize $\text{Li}_{1.0}\text{Ni}_{0.6}\text{Mn}_{0.2}\text{Co}_{0.2}\text{O}_2$ materials, which overcomes the limitations of traditional material synthesis approaches [12]. The proposed method can be operated in a lower temperature environment with respect to the requirements of conventional synthesis methods [12]. The cost-effectiveness, environmental friendliness, and high electrochemical performance makes the newly acquired materials promising candidates to manufacture cathode materials for LIBs.

In the case of anode materials, the most common electrode material for commercial lithium-ion rechargeable batteries is graphite [13]. The advantages of graphite electrodes are low price, large reserves, and high conductivity. However, the disadvantage of the type of material is its low maximum storage capacity (372 mAhg^{-1}) due to the very flat surface and the fact that the charge/discharge rate tends to decrease rapidly after each charge/discharge cycle due to the formation of solid-electrolyte interface (SEI) [14]. Therefore, finding new electrode materials that possess the superior properties of graphite electrodes but can overcome their inherent disadvantages (storage capacity and electron diffusion ability of metal ions) is a major challenge in the lithium-ion rechargeable battery industry.

In 2015, Zhang *et al.* theoretically proposed two-dimensional T12-carbon penta-graphene (PG) as a completely new type of hypothetical carbon material assembled from pentagonal bonds of carbon atoms [15]. These PG sheets have intrinsic indirect bandgap of 3.25 eV, predicted by the Heyd-Scuseria-Ernzerhof (HSE06) exchange-correlation functional, and are thermally stable at temperatures

up to 1000K. In 2016, using density functional theory and molecular dynamics simulations, Xiao *et al.* theoretically showed that albeit penta-graphene sheets are mechanically less stable than graphite monolayers, their maximum storage capacity and average open circuit voltage (OCV) and electron diffusion barrier are 1489 mAhg^{-1} , 0.55 V and 0.17 eV , respectively, making them outstanding candidates for lithium-ion battery cathodes [16]. PG sheets can be cut along a certain crystallographic orientation to create penta-graphene nanoribbons (PGNR). Yuan *et al.* theoretically demonstrated that penta-graphene nanoribbons exhibit a more favorable energetic and thermal stability than armchair and zigzag graphene nanoribbons [17]. Moreover, their stability increases with increasing ribbon width. The ribbons also feature high carrier mobility from $\sim 10^1$ to $\sim 10^4 \text{ cm}^2\text{V}^{-1}\text{s}^{-1}$ at room temperature depending on the edge-terminated atoms [18]. With hydrogen termination at the edges, the PGNR behaves as a semiconductor with a bandgap of 2.4 eV [18] and a low energy diffusion barrier of 0.40 eV [19]. Very recently, Wang *et al.* successfully reduced the diffusion barrier to as low as 0.13 eV reaching the maximum storage capacity of 751 mAhg^{-1} [20] using MoS_2/PG heterostructures.

To boost commercial mobile devices and electric vehicles, besides increasing the storage capacity of the batteries, fast charging capability and longer lifetime are urgently needed. Thus, reducing the energy barrier of lithium-ion diffusion is crucial to improve the electrochemical performance of these fast-growing energy storage devices. Recently, substantial progress has been made to meet these requirements by using novel electrode materials such as MXene [21] or optimizing the electrodes by applying external magnetic [22], [23] or electric fields [24]. Recent experimental reports demonstrate that the charge rates of LIBs can be significantly improved by imposing an external magnetic field parallel to the material surface to reduce the Li-ion transmission paths and increase the diffusion coefficients [23]. Additionally, the charge rates can be easily tuned under external electric fields. For instance, by applying an external electric field on lithium hexafluorophosphate (LiPF_6) in ethylene carbonate, Kumar and Seminario [25] showed a strong impact of the field strength on the electron migration rate of metal ions. Specifically, while the diffusion coefficient increased linearly under a small applied electric field with magnitude below 2 V/nm , it increased exponentially when the electric field strength was above that threshold [25]. Shi *et al.* also showed theoretically that by applying electric fields on MoS_2 monolayers, upon adsorption of Li, Mg, and Al atoms, the electron diffusion barriers decrease while the charge rates of the batteries are accelerated effectively [24]. These results demonstrate the essential role of electric and magnetic fields for improving the migration speed of free electrons for faster and safer charging of LIBs.

Here we employ first principles methods with density functional theory and climbing image-nudged elastic band method to investigate the Li-ion adsorption, electronic properties, and diffusion for PGNR anodes in lithium-ion batteries. We demonstrate the greatly improved electrochemical properties of penta-graphene anodes resulting from the change in structural stability, density of states,

electron diffusion and transition energy under applied electric fields. Such improvement demonstrates the potential application of penta-graphene nanoribbons as anodes for the next generation of lithium-ion rechargeable batteries.

2. Computational methods

In this study, all periodic DFT optimizations were performed using the projector-augmented wave (PAW) method [26] implemented in the Vienna *Ab initio* simulation package (VASP) [27], [28]. We also include the optB86b-vdW [29] exchange-correlation functional in the vdW-DF family to provide reasonable comparison to experimental observations for graphene-like materials [30]. The integration in the Brillouin zone was employed using the Monkhorst-Pack scheme [31] (11 x 1 x 1) with an energy cut-off of 500 eV. The convergence threshold for the self-consistent field calculations was set to 10^{-5} eV per cell, and the geometrical structures were fully optimized until the Hellmann-Feynman forces acting on atoms were less than 0.01 eV \AA^{-1} . To avoid the boundary effect on the interatomic layers of PGNR, a vacuum of 20 \AA is applied between two neighboring nanoribbons.

To determine the most stable of PGNR with a single Li atom, we place the Li atom 3 \AA above the top layer of the PGNR at all possible adsorption sites as shown by letters A-I in Fig. 1(a). The stability of the adsorption configurations is evaluated by the formation energy as follows [32]

$$E_{Form} = \frac{E_{total} - n_C E_C - n_H E_H - n_{Li} E_{Li}}{n_C + n_H + n_{Li}},$$

in which E_{total} is the total Gibbs free energy of the adsorption systems, E_C, E_H, E_{Li} stand for the chemical potentials of C, H, Li atoms. The symbols n_C, n_H, n_{Li} are the number of C, H, Li atoms in the hosted PGNR samples.

To study the electronic properties of the pristine PGNR and the PGNR upon adsorption of lithium-ions at high accuracy, we apply the Heyd-Scuseria-Ernzerhof (HSE06) [33] hybrid functional implemented in the VASP (with the k-point grid of $7 \times 1 \times 1$ in the Monkhorst-Pack scheme) and in the BAND engine of the Amsterdam Modeling Suite (AMS) [34] packages. For the band structure and density of state calculations in the BAND engine, we apply the triple zeta polarization (TZP) basic sets with the core orbitals considered as frozen during the self-consistent field procedure. For further analyses of orbital hybridization, we perform the periodic energy decomposition analyses (PEDA) using the BP86-D3 exchange-correlation potential with the same basic sets in the BAND engine of the AMS package.

The charge/discharge capability is an essential factor to determine whether a proposed material is suitable for developing an anode material for lithium-ion batteries. To characterize the diffusion behavior of lithium ions, we use the climbing image-nudged elastic band (NEB) [35], [36] implemented in the DFTB engine of the AMS package. The initial and final states were taken

systematically from the geometrical optimization procedure in VASP. For each migration path, sixteen intermediate images were used during the NEB image calculations.

3. Results and discussion

3.1 Adsorption of Li-ion on penta-graphene nanoribbons

To evaluate the effect of an external electric field on the electronic and diffusion properties of PGNR upon lithium adsorption, we perform DFT optimization on a PGNR with a width of nine sawtooth carbon chains to obtain the most stable pristine configuration as shown in Fig. 1(a). The C atoms are distributed in three hierarchical atomic planes with a roughness of $d \approx 0.768 \text{ \AA}$. The thickness of these nanoribbons (measured from the top to the bottom layers of C atoms) is $h = 1.412 \text{ \AA}$. There are two types of C-C bonds in the pristine PGNR: C-C single bonds with a length of $\sim 1,504 - 1,569 \text{ \AA}$ and C=C double bonds with a length of $\sim 1,337 - 1,341 \text{ \AA}$. The sp^2 hybridized carbon atoms with three coordination numbers (denoted as C_1 atoms) are located in the middle layer, while the sp^3 carbon atoms with four coordination numbers (C_2) lie in the bottom and top layers (Fig. 1(a)-(c)). These results agree well with previous reports [15], [37], [38]. To further evaluate the stability of PGNR, we also calculate its phonon dispersion spectra. As shown in the phonon spectra of Fig. S1(a), these ribbons are dynamically stable due to the absence of imaginary modes, and we also observe distinct acoustic modes close to the Γ -point, illustrating the typical out-of-plane, in-plane longitudinal, and in-plane transverse atomic motions typical for (penta-)graphene, as thoroughly discussed in Ref. [15].

To investigate the adsorption of Li atoms, we evaluate the structural stability upon adsorption of a single Li atom on nine possible adsorption sites of the most stable PGNR configuration (Fig. 1a). Table 1 presents the formation energy E_{ads} and the corresponding adsorption distances of all possible adsorption sites. The adsorption distance is the center-to-center distance from the adsorbed Li atom to the nearest C atoms of the PGNR. As shown in Table 1, the lowest adsorption energy of all possible adsorption sites is -0.220 eV at the D and E sites. Furthermore, after equilibration, regardless of the initial configurations at D or E sites, the adsorbed Li atom relaxes on top of the sp^3 hybridized C atom, illustrating that the sp^3 configuration is the most energetical stable one. The fundamental phonon dispersion characteristic remains almost unchanged for these nanoribbons upon adsorption of a single Li atom (Fig. S1(b)). Thus, for the further calculations, we associate the PGNR with a Li atom on top of the sp^3 C atom as the most stable configuration.

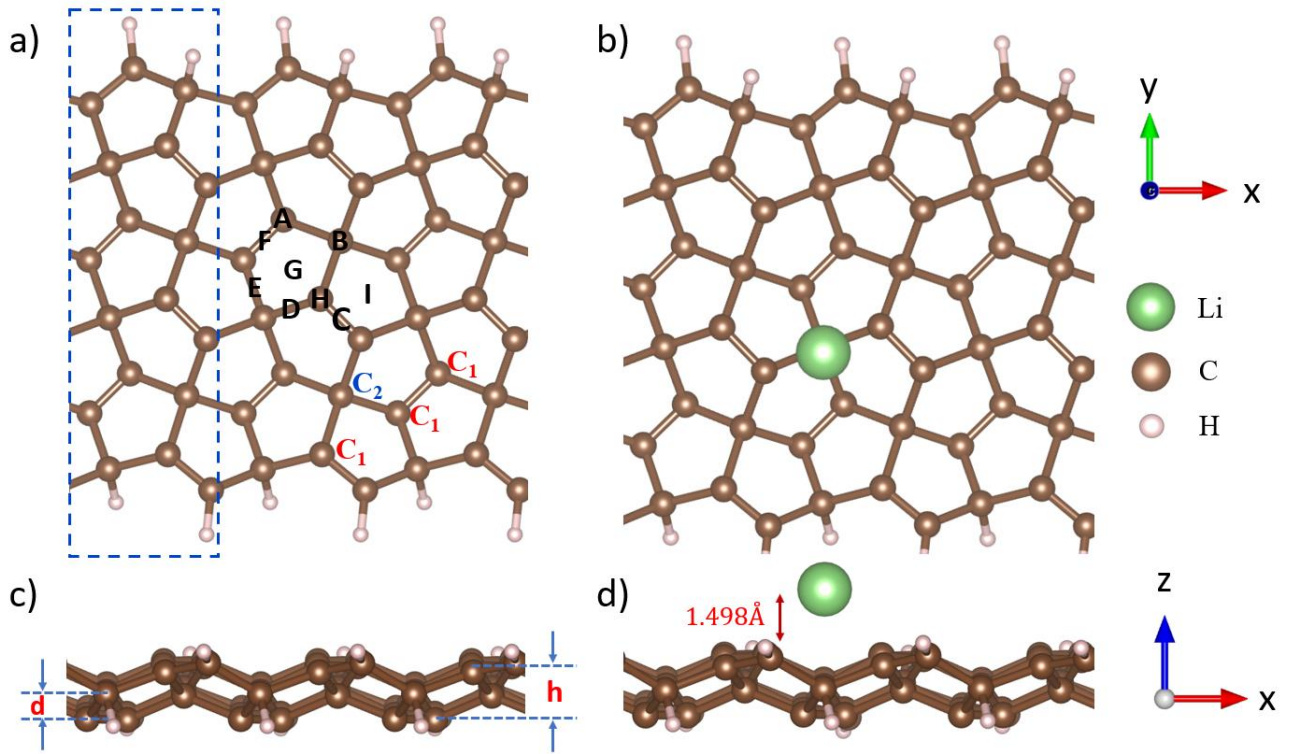


Figure 1. Top- and side-view of the optimized geometrical structures of PGNR (ac) and PGNR + Li (bd). The yellow, gray and white balls illustrate Li, C and H atoms, respectively. The possible Li adsorption sites (a) are marked as on top (A, B, H), at hollow (I, G), and in the bridge (C, D, E, F) of C atoms. The dashed blue rectangle represents the supercell of PGNR.

Table 1. Formation energies E_{ads} and adsorption distances a from the Li atom to PGNR at different adsorption sites.

Site	A	B	C	D	E	F	G	H	I
E_{ads} (eV)	-0.219	-0.219	-0.216	-0.220	-0.220	-0.219	-0.218	-0.218	-0.219
a (Å)	1.345	1.444	1.943	1.498	1.491	1.014	1.026	1.031	1.148

Table 2. The structural modification of the PGNR under an applied electric field.

Electric field strength (V/nm)	-2	-1	0	1	2
Relative energy difference (eV)	-0.018	-0.162	0	-0.084	-0.169
Lattice constant in x-direction (Å)	10.854	10.854	10.857	10.854	10.855
Buckling distance (Å)	0.642	0.743	0.677	0.712	0.667

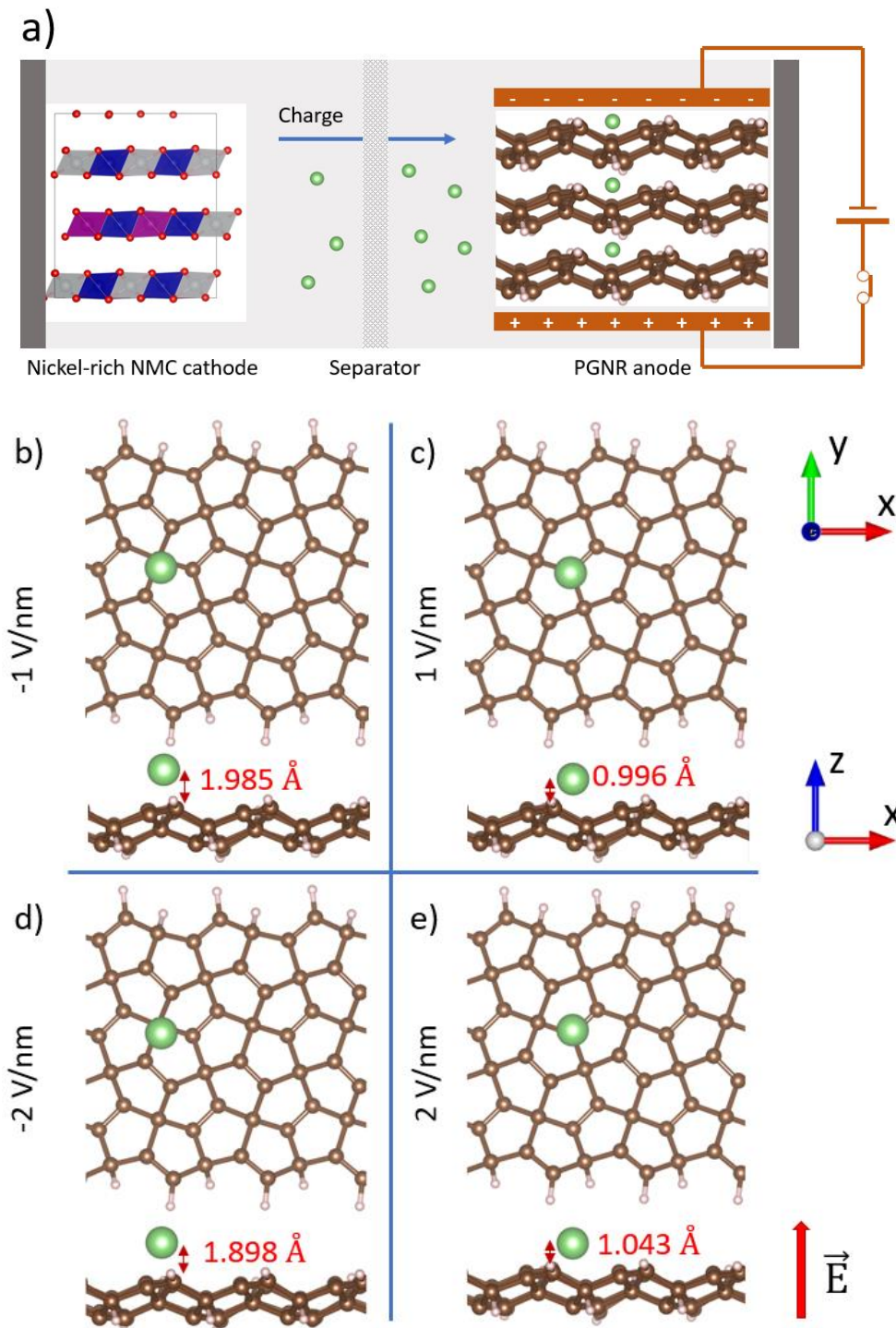


Figure 2. (a) Sketch of a lithium-ion battery with a penta-graphene nanoribbon anode under a vertical electric field. The geometrical structures with top and side views of these adsorbed system under an electric field of -1V/nm (b), 1 V/nm (c), -2 V/nm (d) and 2 V/nm (e). The positive direction of the external electric field is sketched at the bottom right of figure (e). The shortest distances from the adsorbed lithium-ion to PGNR are also displayed in these figures.

We now apply an electric field perpendicular to these nanoribbons. The strength of the applied field varies from -2 V/nm to 2 V/nm with a stepsize of 1 V/nm, where positive (negative) values indicate a field in the positive (negative) z-direction. This field is strong enough to disturb the electron diffusion

process but is weak enough not to destroy the adsorption system. Under a positive electric field, the adsorbed Li atom relaxes on top of the sp^2 hybridized carbon atom as indicated in Fig. 2. However, under a negative electrical field, the adsorbed Li atom anchors close to the top of the sp^3 hybridized carbon atom. To evaluate the stability of these configurations, we calculate the relative energy difference, which is the energy difference between the systems with the electric field and the one without. As shown in Table 2, the adsorption systems are slightly more stable with applied electric field than without, as indicated by the negative values of the relative energy difference. Apart from that, the lattice constant in the x-direction and the buckling amplitude of the systems show minor changes with the largest buckling of 9.75%. Though there is a presence of a negative dispersion band when these nanoribbons are under a positive electric field (Fig. S1(c-d)), in general, these ribbons are mechanically stable under these small electric fields. The most interesting observation is that the Li atom is adsorbed more closely to the PGNR when a positive electric field is applied. As shown in Fig. 2, the adsorption distance from the Li atom to the PGNR reduces by about 30% when the field is applied in the z-direction, while for fields in the opposite direction, this quantity extends by about 30% with respect to the field-less case. This implies significant changes of the electronic transport properties as discussed in the next section.

3.2 Effects of an electric field on the electronic properties of Li-ion penta-graphene nanoribbons

To increase the accuracy as well as the reliability of the calculated electronic properties, we further calculate the band structure and partial density of states of these adsorbed systems using the state-of-art HSE06 hybrid functionals [39]. As shown in Figs. 3 and S2-S3, the PGNR exhibits semiconductor properties with an indirect bandgap of 3.415 eV or 3.433 eV, as calculated by the AMS and VASP packages, respectively. These results are in quantitative agreement with the previous report of 3.25 eV [15] for a two-dimensional penta-graphene system. The electronic energy states are mainly dominated by the $2-p_z$ orbitals of carbon atoms (Fig. S3), illustrating the high possibility for orbital hybridization in the z direction. The localized π electrons of sp^2 carbon atoms are also well visualized by the shapes of frontier orbitals (both the highest occupied molecular orbital (HOMO) and the lowest unoccupied molecular orbital (LUMO) states) on the top-left of Table S1, which is typical for penta-graphene nanoribbons [40].

Upon lithium adsorption, the semiconductor PGNR becomes metal as indicated in Fig. 4, in line with previous reports [15], [41]. This semiconductor-to-metal transition demonstrates that PGNR is a good anode material for lithium-ion batteries due to creation of free charges from the interaction between the adsorbed Li atoms and C atoms of the PGNR. The energy states around the Fermi level are driven by the π electrons of carbon atoms as displayed in Fig. S4, demonstrating a charge transfer from the adsorbed Li atom to the PGNR as pointed out in Ref. [41] and a high possibility of

hybridization between p -orbital of the C and s -orbital. These electrons occupy the energy levels from 0.6 to up (HSE06) with respect to the lowest unoccupied molecular orbital (LUMO). The filled of the s -orbital of the Li atom at the states close to the Fermi level with significant DOS indicates the increase of the conductivity of PGNR upon adsorption of Li atoms, leading to the semiconductor-to-metal transition. Additionally, the interaction with the Li atom can enhance the flexibility of p -orbital electrons of the C atoms, leading to a strong shifting of the highest occupied molecular orbital (HOMO) up to the bottom of the conduction band (see Figs. 4 and 5S). The electrons transferred from the Li and the flexible p -orbital electrons of the C occupied the HOMO play an important role to increase the conductivity of Li + PGNR.

Figure 4 displays a significant band modification of the PGNR + Li under an external electric field. Under a 2 V/nm electric field, we observe a considerable down-shifted band dispersion curves in the conduction band towards the Fermi level while this trend is less pronounced in the case of a -2 V/nm electric field. Similar behavior is also observed in Fig. S4 obtained from the VASP package. Moreover, there is a noticeable increase of the pDOS at the Fermi level under the negative electric field while under the positive electric field, these partial densities are almost equivalent to those of zero applied field. The increase of the of the pDOS at the Fermi level under the negative electric field indicates implies the increase of the conductivity when applied the weak negative electric field. Under the positive external electric field, there is the additional appearance of a new state in the conduction band lying just above the Fermi level. This state is occupied by s -orbital of the adsorbed Li atoms with higher density compared to the nearby states in the conduction band as indicated in Fig. S4. It demonstrates the increase of the conductivity of PGNR + Li under the positive external electric field. Note that the modifications of the band structure and DOS of PGNR + Li under the positive external electric field are different from those under the negative external electric field. It is equivalent that the electronic characteristics of the PGNR + Li strongly depend on the direction of the applied external electric field.

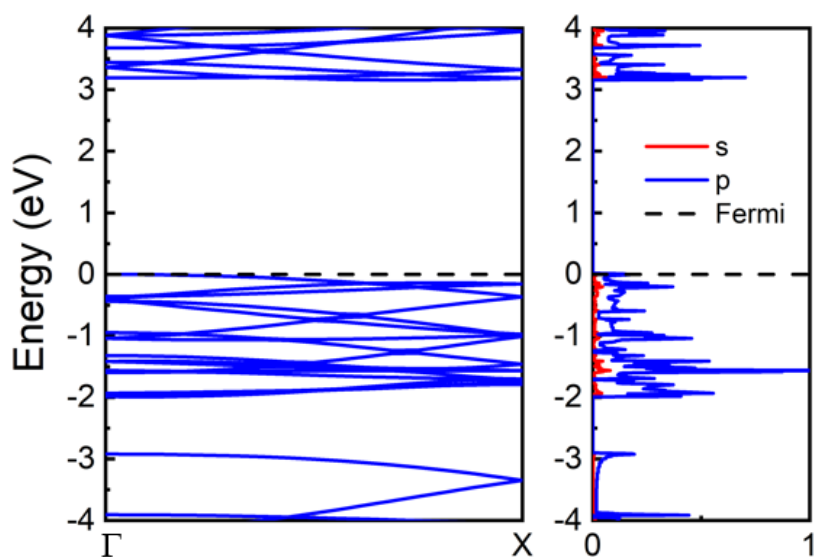


Figure 3. Band structure and partial density of states of penta-graphene nanoribbons calculated by the HSE06 hybrid functional implemented in the AMS package. The Fermi level is indicated by the dashed lines.

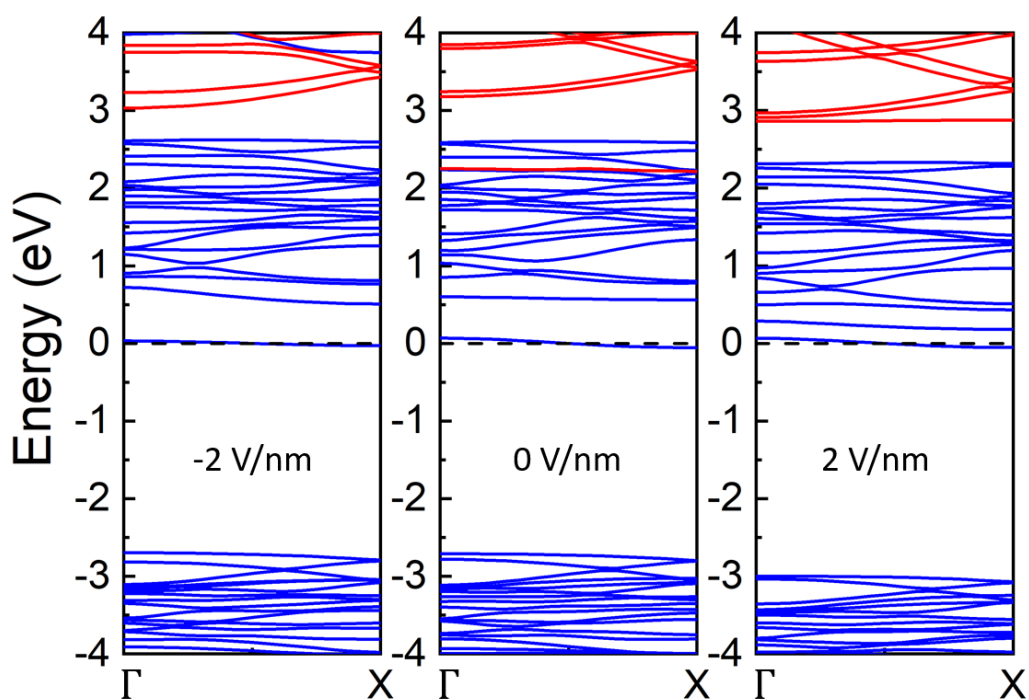


Figure 4. Band structure of penta-graphene nanoribbons upon adsorption of a lithium atom calculated by the hybrid HSE06 functional implemented in the AMS package. Red and blue lines represent for the s- and p-orbitals. The Fermi level is indicated by the dashed lines.

Upon adsorption of a single Li atom, the distribution of electrons of the HOMO and LUMO exhibits a higher localization. They mainly concentrate on the top of C atoms near the adsorbed Li atom with relative high density and could act as free electrons, leading to the increase of the conductivity of PGNR upon adsorption of the Li atom. Such a redistribution of electrons of the frontier orbitals due to the Li adsorption also results the transition from the conductor-to-metal behavior of PGNR. When a weak external electric field is applied, although the orbital shape of the LUMO of the PGNR+ Li exhibits an inconsiderable change, the orbital shape of the LUMO modifies significantly as shown in Table 3. The electrons of the LUMO distribute more locally under the effect of the external electric field and their density on the top of the C atoms around the adsorbed Li atom is found to increase. The electrons of the LUMO even surround the Li atom as applied the negative external electric field. Such change of the LUMO orbital shape implies a strong increase of the conductivity of PGNR + Li under the external electric field, in good agreement with the increasing of the DOS of the LUMO shown in Fig. S5. Interestingly, Table 3 also shows that under an effect of a negative external electrical field, the electron depletion areas of the frontier orbitals are replaced by the accumulation areas, whereas this phenomenon is not observed as applying a positive external electrical field, demonstrating the dependence of electronic properties of the PGNR + Li on the direction of the applied electrical field.

Table 3. Shapes of frontier orbitals of PGNR, PGNR + Li in the absence of and under an external electric field in top- (upper images) and side- (lower images) views. Iso-value for the orbital rendering is $0.02 \text{ eV}/\text{\AA}^2$. The electron depletion is in blue whereas the electron accumulation is in reddish brown.

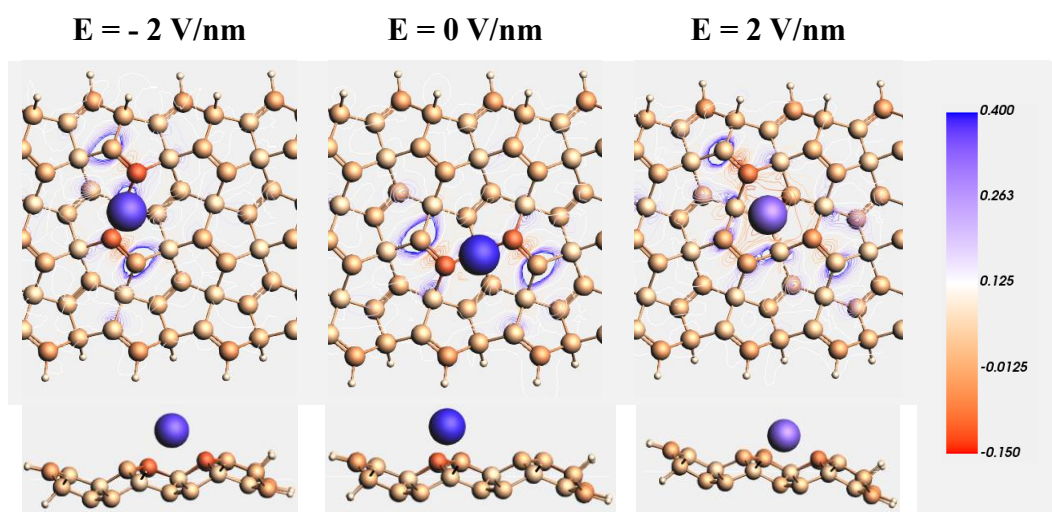


Table 4. Periodic energy decomposition analyses (PEDA) of PGNR upon adsorption of a Li atom. All units are in kJ mol^{-1} .

PEDA types	E = - 2 V/nm	E = 0 V/nm	E = 2 V/nm
ΔE_{int}	-41.9	-64.9	-62.2
ΔE_{elstat}	-318.5	-418.3	-670.2
ΔE_{orb}	-183.0	-249.4	-367.6

To further understand the influence of weak external electric field of the electronic properties of PGNR + Li, we performed periodic energy decomposition analyses (PEDA) to calculate the intrinsic bond energies ΔE_{int} and their partial energies. It notes that

$$\Delta E_{int} = \Delta E_{elstat} + \Delta E_{Pauli} + \Delta E_{orb},$$

where ΔE_{elstat} , ΔE_{Pauli} , and ΔE_{orb} are the electrostatic energy, the Pauli repulsion energy, and the orbital relaxation energy of the adsorption system, respectively. Table 5 displays the obtained intrinsic bond energies and partial periodic energies of PGNR upon adsorption of a Li atom without and with the presence of the external electrical field. It can find that a weak external electrical field can modify the intrinsic bond energies and their partial parts, *i.e.*, modifying the interaction between PGNR and Li. However, the weak external electrical field does not change the intrinsic interaction nature between PGNR and Li atom. In more details, the electrostatic energy part plays the most dominant factor in the absence or presence of the external electrical field, illustrating that the interaction between PGNR and Li is mainly driven by the electrostatic effect and the adsorbed Li atoms donate a considerable charge amount to the PGNR. It also proves the metal nature of the PGNR + Li. We also pay a great of attention on the orbital relaxation energies, which cover the orbital hybridization effect in the adsorption system. The magnitudes of both the electrostatic and the orbital relaxation energy parts remarkably decrease as introducing the negative external electrical field but they significantly increase as applying the negative external electrical field, indicating the electronic property dependence of the PGNR + Li on the direction of the external electrical field. The increase of electrostatic energy magnitude totally corresponds to the strong charge redistribution of the frontier orbital and the nearby states shown in Table 4 and Figs. S4-S5 under the effect of the positive external electrical field. Moreover, it

demonstrates that the charge distribution of the adsorbent and the adsorbate is denser due to increase of the charge transfer as reducing the shortest distance between the Li and the PGNR pointed out above. As a result, the diffusion coefficient of Li ions on PGNR under the positive external electrical field is significantly higher than that under the negative external electrical field as well without external electrical field. Corresponding to the reduction of the orbital relaxation energy under the negative external electrical field, the orbital hybridization between the adsorbed Li and the PGNR is weakened. Therefore, the flexibility of the *p*-orbital electrons of the C atoms is enhanced. Therefore, the conductivity of the PGNR + Li as well as the diffusion coefficient of Li ions on PGNR increase.

3.3 Effects of an electric field on the diffusion process of Li-ion penta-graphene nanoribbons

The diffusion energy profiles and the energy barriers of lithium-ion migration are an essential factor for evaluating the performance of lithium-ion anodes. The low energy barriers indicate that the lithium-ions can easily migrate along preferable diffusion paths. In this section, we investigate the effect of an external electric field on the lithium-ion diffusion characteristics of penta-graphene nanoribbons. As discussed above, under a zero and negative electric fields, the adsorbed lithium atoms are energetically stable on top of the *sp*³ hybridized carbon atoms while under the positive fields, the equivalent stabilized positions are on top of the *sp*² carbon atoms. The diffusion paths are chosen as the shortest paths between the two most energetically favorable configurations as illustrated by red arrows in Fig. 5. In the absence of an electric field, the diffusion barrier calculated by the CI-NEB method along the diffusion path highlighted in Fig. 5(a) is 0.272 eV, which is in quantitative agreement with that of two-dimensional penta-graphene (≤ 0.33 eV) [16], comparable to the case of penta-hexagonal graphene (in between 0.21 eV and 0.32 eV) [43] and significantly lower than those of commercial graphite anodes (0.4-0.6 eV) [43] and LiFePO₄ (1.02 eV) electrodes [44]. In the presence of an external electric field, this diffusion barrier significantly reduces to the lowest value of ~ 0.1 eV at 2 V/nm electric field as shown in Table 5 and Fig. 5. Such low diffusion barrier, which is comparable with that of Ti₃C₂ [43] and the recent proposed MoS₂/penta-graphene heterostructures [20], strongly demonstrates the remarkable fast ion diffusion of penta-graphene nanoribbons under an applied electric field.

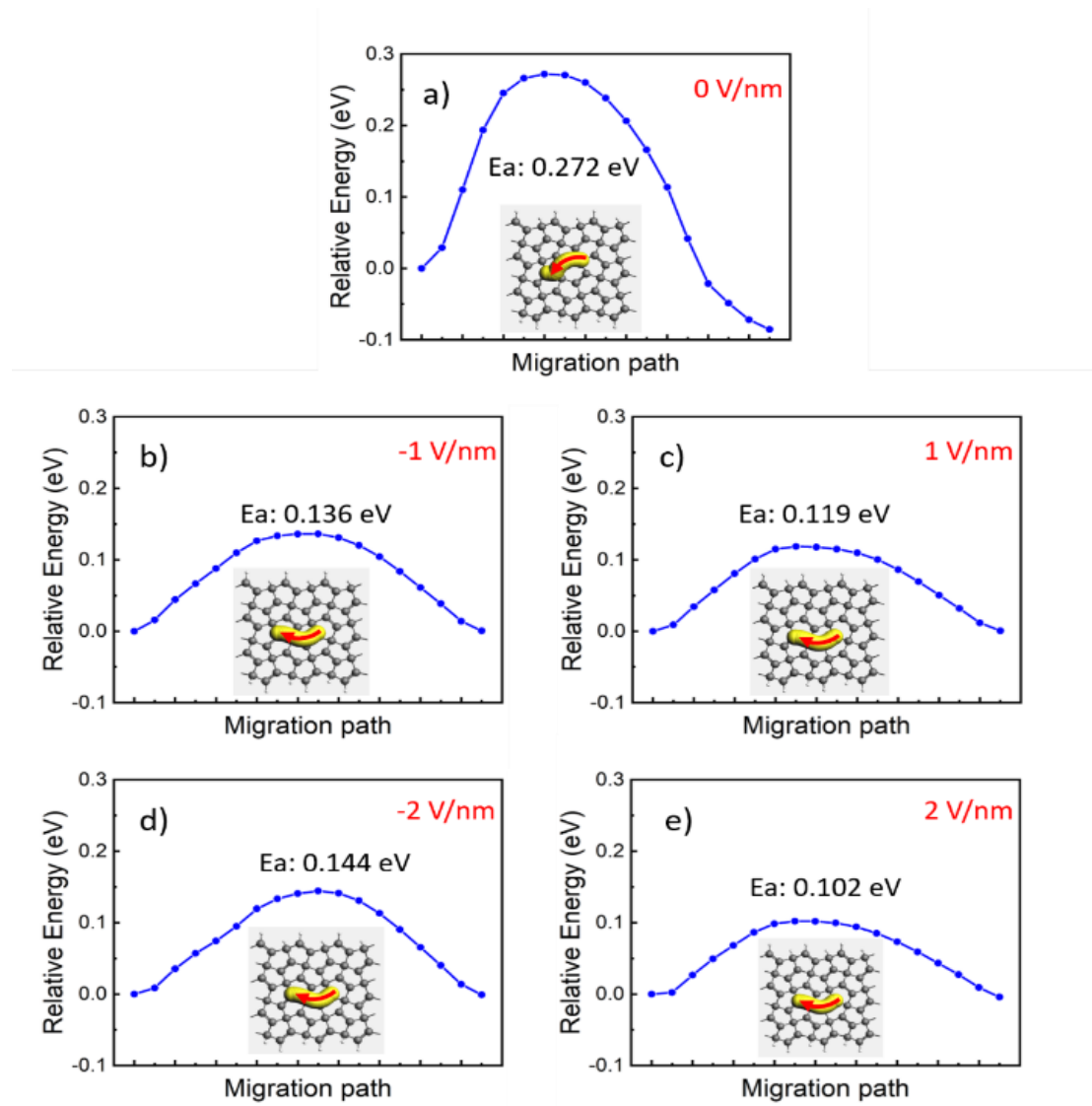


Figure 5. Diffusion barriers of lithium-atoms on penta-graphene nanoribbons under an external electric field.

Table 5. Diffusion barrier and diffusion coefficient of lithium-ions on penta-graphene nanoribbons under an external electric field.

Electric field strength (V/m)	-2	-1	0	1	2
Diffusion barrier (eV)	0.144	0.13617	0.272	0.119	0.102
Diffusion coefficient (cm ² /s)	4.5×10^{-4}	6.2×10^{-4}	3.2×10^{-6}	1.2×10^{-3}	2.3×10^{-3}
The lithium diffusion coefficient ratio between penta-graphene nanoribbons and graphitic carbon	102.78	139.99	0.73	269.98	520.71

[45]

The diffusion coefficient of lithium-ions can be calculated via the relation $D = a^2 \nu e^{-\frac{E_{act}}{k_B T}}$, where a is the diffusion length of ions, $\nu \sim 10^{13} \text{ Hz}$, k_B is Boltzmann's constant, T is the room temperature ($T = 300 \text{ K}$) [44], and E_{act} stands for the diffusion barrier. As shown in Table 5, in the absence of an electric field, the lithium-ion diffusion coefficient of penta-graphene nanoribbons is $3.2 \times 10^{-6} \text{ cm}^2/\text{s}$ while under an external electric field, this diffusion coefficient increases significantly. Specifically, under a positive electric field of 1 V/nm and 2 V/nm, it reaches to $1.2 \times 10^{-3} \text{ cm}^2/\text{s}$ and $2.3 \times 10^{-3} \text{ cm}^2/\text{s}$, which is approximately about 369 and 711 times faster than that of the case of zero electric field, respectively. Under negative electric fields, though we also observe an increase of diffusion coefficients, these quantities are relatively smaller than in the case of positive electric fields. These observations are in line with the additional electronic states formed in the conduction bands close to the Fermi level (Figs. S4 and S5). To demonstrate the outperformance of PGNR as a promising material for lithium-ion anodes, we compare our calculated diffusion coefficients with those of carbon graphite layer, a common electrode material in recent commercial batteries [45]. Table 5 illustrates that the diffusion coefficient of PGNR under a zero electric field is slightly lower than that of graphitic carbon layers in the direction parallel to graphene planes and this quantity reaches ~ 520 times higher under a 2 V/nm electric field. Therefore, the external electric field can be used as a novel switch to remarkably improve the charge/discharge rate of penta-graphene lithium-ion anodes.

Besides the diffusion barriers and diffusion coefficients, another essential factor which greatly contributes to the charge/discharge rates of lithium-ion anodes is the electronic conductivity, which can be inferred by carrier effective mass [46]. The effective masses of electrons (m_e^*) and holes (m_h^*) are calculated from $m^* = \hbar^2 \left(\frac{d^2 E(k)}{dk^2} \right)^{-1}$ equation, where \hbar is the Planck's constant, k and $E(k)$ are respectively the wave vector and the energy dispersion relation corresponding to the conduction-band minima and valence-band maxima [44] of Figs. 3 and 4. The effective masses of holes and electrons of pristine PGNR are $0.852m_0$ and $0.519m_0$ (where m_0 is the mass of an electron), respectively, which are larger than the effective masses of holes and electrons in two-dimensional penta-graphene ($0.50m_0$ and $0.24m_0$, respectively [47]). These results indicate that holes and electrons of pristine penta-graphene nanoribbons are less mobile than those of penta-graphene monolayers. Upon adsorption of a single Li atom, the effective mass of electrons is $1.442m_0$ which is ~ 2.8 times higher than that of pristine PGNR and the m_h^*/m_e^* is 0.584, meaning that these electrons are even less mobile than in the case of pristine systems. However, under an external electric field, these m_h^*/m_e^* effective mass ratios increase dramatically. While in the negative electric fields, these ratios increase a few times, in the opposite electric field directions, we observe remarkable increases up to ~ 26 times higher (see Table 6). Obviously, this sudden increase of the m_h^*/m_e^* ratios highlight the role of an external electric field as a novel switch to improve the conductivity of penta-graphene lithium-ion anodes.

Table 6. Effective masses of electrons (m_e^*/m_0) and holes (m_h^*/m_0) of penta-graphene nanoribbons upon adsorption of lithium-ions under an external electric field.

Electric field (V/nm)	-2	-1	0	1	2
m_h^*/m_0	0.865	0.863	0.842	0.864	0.865
m_e^*/m_0	0.217	0.145	1.442	0.036	0.033
m_h^*/m_e^*	3.986	5.952	0.584	24.000	26.212

4. Conclusions

We have presented in detail the remarkable role of an external electric field to enhance the electronic properties and the diffusion of lithium-ions of penta-graphene nanoribbons upon adsorption of lithium atoms. We show that the adsorbed systems are as thermodynamically stable as the pristine systems. After adsorbing lithium atoms, the semiconductor penta-graphene nanoribbons become metal, originating from the orbital hybridization between the sp^3 carbon atoms and the lithium atoms. When used as lithium-ion anode materials, PGNR exhibit fast diffusion coefficient of PGNR of 3.7×10^5 times higher than that of carbon graphite layer. The external electric field can be used a novel switch to improve the efficiency of lithium-ion batteries with penta-graphene nanoribbon anodes. Furthermore, these electric fields support directional orientations of electron conductivity and diffusions, and penta-graphene nanoribbons promise an excellent anode material for lithium-ion batteries with ultrafast charge/discharge rates.

Conflicts of interest

There are no conflicts to declare.

Acknowledgements

The authors acknowledge the Information and Network Management Centre at Can Tho University for providing high-performance computing resources.

References

- [1] “Lithium-ion batteries - statistics & facts | Statista.” Accessed: Aug. 12, 2023. [Online]. Available: <https://www.statista.com/topics/2049/lithium-ion-battery-industry/#topicOverview>
- [2] W. Zuo, A. Innocenti, M. Zarrabeitia, D. Bresser, Y. Yang, and S. Passerini, “Layered Oxide Cathodes for Sodium-Ion Batteries: Storage Mechanism, Electrochemistry, and Techno-economics,” *Acc Chem Res*, vol. 56, no. 3, pp. 284–296, Feb. 2023, doi: 10.1021/acs.accounts.2c00690.

- [3] K. Ozawa, "Lithium-ion rechargeable batteries with LiCoO₂ and carbon electrodes: the LiCoO₂/C system," *Solid State Ion*, vol. 69, no. 3, pp. 212–221, 1994, doi: [https://doi.org/10.1016/0167-2738\(94\)90411-1](https://doi.org/10.1016/0167-2738(94)90411-1).
- [4] Y. Lyu *et al.*, "An Overview on the Advances of LiCoO₂ Cathodes for Lithium-Ion Batteries," *Adv Energy Mater*, vol. 11, no. 2, p. 2000982, Jan. 2021, doi: <https://doi.org/10.1002/aenm.202000982>.
- [5] X. Zhu *et al.*, "LiMnO₂ cathode stabilized by interfacial orbital ordering for sustainable lithium-ion batteries," *Nat Sustain*, vol. 4, no. 5, pp. 392–401, 2021, doi: 10.1038/s41893-020-00660-9.
- [6] H. Zhao *et al.*, "Orthorhombic LiMnO₂ nanorods as cathode materials for lithium-ion batteries: Synthesis and electrochemical properties," *Ceram Int*, vol. 42, no. 7, pp. 9319–9322, 2016, doi: <https://doi.org/10.1016/j.ceramint.2016.01.207>.
- [7] Y. Zhang *et al.*, "Advances in new cathode material LiFePO₄ for lithium-ion batteries," *Synth Met*, vol. 162, no. 13, pp. 1315–1326, 2012, doi: <https://doi.org/10.1016/j.synthmet.2012.04.025>.
- [8] S.-P. Chen, D. Lv, J. Chen, Y.-H. Zhang, and F.-N. Shi, "Review on Defects and Modification Methods of LiFePO₄ Cathode Material for Lithium-Ion Batteries," *Energy & Fuels*, vol. 36, no. 3, pp. 1232–1251, Feb. 2022, doi: 10.1021/acs.energyfuels.1c03757.
- [9] R. Jung, M. Metzger, F. Maglia, C. Stinner, and H. A. Gasteiger, "Chemical versus Electrochemical Electrolyte Oxidation on NMC111, NMC622, NMC811, LNMO, and Conductive Carbon," *J Phys Chem Lett*, vol. 8, no. 19, pp. 4820–4825, Oct. 2017, doi: 10.1021/acs.jpcclett.7b01927.
- [10] R. Tatara *et al.*, "Enhanced Cycling Performance of Ni-Rich Positive Electrodes (NMC) in Li-Ion Batteries by Reducing Electrolyte Free-Solvent Activity," *ACS Appl Mater Interfaces*, vol. 11, no. 38, pp. 34973–34988, Sep. 2019, doi: 10.1021/acsami.9b11942.
- [11] M. Malik, K. H. Chan, and G. Azimi, "Review on the synthesis of LiNi_xMn_yCo_{1-x-y}O₂ (NMC) cathodes for lithium-ion batteries," *Mater Today Energy*, vol. 28, p. 101066, 2022, doi: <https://doi.org/10.1016/j.mtener.2022.101066>.
- [12] T. Le Thi *et al.*, "Modified Coprecipitation Synthesis of Nickel-Rich NMC (Li_{1.0}Ni_{0.6}Mn_{0.2}Co_{0.2}O₂) for Lithium-Ion Batteries: A Simple, Cost-Effective, Environmentally Friendly Method," *ACS Omega*, vol. 8, no. 48, pp. 45414–45427, Dec. 2023, doi: 10.1021/acsomega.3c04717.
- [13] H. Zhang, Y. Yang, D. Ren, L. Wang, and X. He, "Graphite as anode materials: Fundamental mechanism, recent progress and advances," *Energy Storage Mater*, vol. 36, pp. 147–170, 2021, doi: <https://doi.org/10.1016/j.ensm.2020.12.027>.
- [14] R. Fang, K. Chen, L. Yin, Z. Sun, F. Li, and H. M. Cheng, "The Regulating Role of Carbon Nanotubes and Graphene in Lithium-Ion and Lithium–Sulfur Batteries," *Advanced Materials*, vol. 31, no. 9, p. 1800863, Mar. 2019, doi: 10.1002/ADMA.201800863.

- [15] S. Zhang, J. Zhou, Q. Wang, X. Chen, Y. Kawazoe, and P. Jena, "Penta-graphene: A new carbon allotrope," *Proc Natl Acad Sci U S A*, vol. 112, no. 8, pp. 2372–2377, Feb. 2015, doi: 10.1073/PNAS.1416591112.
- [16] B. Xiao, Y. chun Li, X. fang Yu, and J. bo Cheng, "Penta-graphene: A Promising Anode Material as the Li/Na-Ion Battery with Both Extremely High Theoretical Capacity and Fast Charge/Discharge Rate," *ACS Appl Mater Interfaces*, vol. 8, no. 51, pp. 35342–35352, Dec. 2016, doi: 10.1021/ACSAMI.6B12727.
- [17] P. F. Yuan, Z. H. Zhang, Z. Q. Fan, and M. Qiu, "Electronic structure and magnetic properties of penta-graphene nanoribbons," *Physical Chemistry Chemical Physics*, vol. 19, no. 14, pp. 9528–9536, 2017, doi: 10.1039/C7CP00029D.
- [18] Y. H. Li, P. F. Yuan, Z. Q. Fan, and Z. H. Zhang, "Electronic properties and carrier mobility for penta-graphene nanoribbons with nonmetallic-atom -terminations," *Org Electron*, vol. 59, pp. 306–313, 2018, doi: <https://doi.org/10.1016/j.orgel.2018.05.039>.
- [19] U. Palanivel, H.-K. Kim, and Y.-C. Kim, "Adsorption and Migration of a Single Lithium on Tetra-Penta-Hepta-Graphene Nanoribbon: a Density Functional Theory Approach," *physica status solidi (b)*, vol. 259, no. 3, p. 2100369, Mar. 2022, doi: <https://doi.org/10.1002/pssb.202100369>.
- [20] T. Wang *et al.*, "First-principles study of penta-graphene/MoS₂ vdW heterostructure as anode material for lithium-ion batteries," *Diam Relat Mater*, vol. 136, p. 109928, 2023, doi: <https://doi.org/10.1016/j.diamond.2023.109928>.
- [21] Y. Xia *et al.*, "Tailoring Nitrogen Terminals on MXene Enables Fast Charging and Stable Cycling Na-Ion Batteries at Low Temperature," *Nanomicro Lett*, vol. 14, no. 1, p. 143, 2022, doi: 10.1007/s40820-022-00885-7.
- [22] G. Ruan, J. Hua, X. Hu, and C. Yu, "Study on the influence of magnetic field on the performance of lithium-ion batteries," *Energy Reports*, vol. 8, pp. 1294–1304, 2022, doi: <https://doi.org/10.1016/j.egy.2022.02.095>.
- [23] L. Zhang, M. Zeng, D. Wu, and X. Yan, "Magnetic Field Regulating the Graphite Electrode for Excellent Lithium-Ion Batteries Performance," *ACS Sustain Chem Eng*, vol. 7, no. 6, pp. 6152–6160, Mar. 2019, doi: 10.1021/acssuschemeng.8b06358.
- [24] W. Shi, Z. Wang, Z. Li, and Y. Q. Fu, "Electric field enhanced adsorption and diffusion of adatoms in MoS₂ monolayer," *Mater Chem Phys*, vol. 183, pp. 392–397, 2016, doi: <https://doi.org/10.1016/j.matchemphys.2016.08.043>.
- [25] N. Kumar and J. M. Seminario, "Lithium-ion model behavior in an ethylene carbonate electrolyte using molecular dynamics," *Journal of Physical Chemistry C*, vol. 120, no. 30, pp. 16322–16332, Aug. 2016, doi: 10.1021/ACS.JPCC.6B03709.
- [26] G. Kresse and D. Joubert, "From ultrasoft pseudopotentials to the projector augmented-wave method," *Phys. Rev. B*, vol. 59, no. 3, pp. 1758–1775, Jan. 1999, doi: 10.1103/PhysRevB.59.1758.

- [27] G. Kresse and J. Hafner, "Ab initio molecular-dynamics simulation of the liquid-metalamorphous- semiconductor transition in germanium," *Phys Rev B*, vol. 49, no. 20, pp. 14251–14269, 1994, doi: 10.1103/PhysRevB.49.14251.
- [28] G. Kresse and J. Furthmüller, "Efficiency of ab-initio total energy calculations for metals and semiconductors using a plane-wave basis set," *Comput Mater Sci*, vol. 6, no. 1, pp. 15–50, 1996, doi: [https://doi.org/10.1016/0927-0256\(96\)00008-0](https://doi.org/10.1016/0927-0256(96)00008-0).
- [29] S. Grimme, J. Antony, S. Ehrlich, and H. Krieg, "A consistent and accurate ab initio parametrization of density functional dispersion correction (DFT-D) for the 94 elements H-Pu," *J Chem Phys*, vol. 132, no. 15, p. 154104, Apr. 2010, doi: 10.1063/1.3382344.
- [30] M.-S. Zheng, S. Zhou, X. Wang, and L. Gao, "Understanding epitaxy of graphene: From experimental observation to density functional theory and machine learning," *J Appl Phys*, vol. 134, no. 9, p. 090901, Sep. 2023, doi: 10.1063/5.0163580.
- [31] H. J. Monkhorst and J. D. Pack, "Special points for Brillouin-zone integrations," *Phys. Rev. B*, vol. 13, no. 12, pp. 5188–5192, Jun. 1976, doi: 10.1103/PhysRevB.13.5188.
- [32] E. Perim, R. Paupitz, P. A. S. Autreto, and D. S. Galvao, "Inorganic Graphenylene: A Porous Two-Dimensional Material With Tunable Band Gap," *The Journal of Physical Chemistry C*, vol. 118, no. 41, pp. 23670–23674, Oct. 2014, doi: 10.1021/jp502119y.
- [33] K. Lee, É. D. Murray, L. Kong, B. I. Lundqvist, and D. C. Langreth, "Higher-accuracy van der Waals density functional," *Phys Rev B*, vol. 82, no. 8, p. 81101, Aug. 2010, doi: 10.1103/PhysRevB.82.081101.
- [34] C. J. O. Verzijl and J. M. Thijssen, "DFT-Based Molecular Transport Implementation in ADF/BAND," *The Journal of Physical Chemistry C*, vol. 116, no. 46, pp. 24393–24412, Nov. 2012, doi: 10.1021/jp3044225.
- [35] G. Henkelman, B. P. Uberuaga, and H. Jónsson, "A climbing image nudged elastic band method for finding saddle points and minimum energy paths," *J Chem Phys*, vol. 113, no. 22, pp. 9901–9904, Dec. 2000, doi: 10.1063/1.1329672.
- [36] G. Henkelman and H. Jónsson, "Improved tangent estimate in the nudged elastic band method for finding minimum energy paths and saddle points," *Journal of Chemical Physics*, vol. 113, no. 22, pp. 9978–9985, Dec. 2000, doi: 10.1063/1.1323224.
- [37] B. Rajbanshi, S. Sarkar, B. Mandal, and P. Sarkar, "Energetic and electronic structure of penta-graphene nanoribbons," *Carbon N Y*, vol. 100, pp. 118–125, Apr. 2016, doi: 10.1016/J.CARBON.2016.01.014.
- [38] T. Y. Mi, D. M. Triet, and N. T. Tien, "Adsorption of gas molecules on penta-graphene nanoribbon and its implication for nanoscale gas sensor," *Physics Open*, vol. 2, Mar. 2020, doi: 10.1016/J.PHYSO.2020.100014.
- [39] A. V Krukau, O. A. Vydrov, A. F. Izmaylov, and G. E. Scuseria, "Influence of the exchange screening parameter on the performance of screened hybrid functionals," *J Chem Phys*, vol. 125, no. 22, p. 224106, Dec. 2006, doi: 10.1063/1.2404663.

- [40] B. Rajbanshi, S. Sarkar, B. Mandal, and P. Sarkar, "Energetic and electronic structure of penta-graphene nanoribbons," *Carbon N Y*, vol. 100, pp. 118–125, 2016, doi: <https://doi.org/10.1016/j.carbon.2016.01.014>.
- [41] S. Li, Y. Shen, D. Ni, and Q. Wang, "A new 3D metallic carbon allotrope composed of penta-graphene nanoribbons as a high-performance anode material for sodium-ion batteries," *J Mater Chem A Mater*, vol. 9, no. 40, pp. 23214–23222, 2021, doi: 10.1039/D1TA07000B.
- [42] D. Krepel and O. Hod, "Lithium adsorption on armchair graphene nanoribbons," *Surf Sci*, vol. 605, no. 17, pp. 1633–1642, 2011, doi: <https://doi.org/10.1016/j.susc.2010.11.019>.
- [43] L. Lu, R. Gallenstein, X. Liu, Y. Lin, S. Lin, and Z. Chen, "Holey penta-hexagonal graphene: a promising anode material for Li-ion batteries," *Phys. Chem. Chem. Phys.*, vol. 26, no. 9, pp. 7335–7342, 2024, doi: 10.1039/D3CP06146A.
- [44] Z. Cui *et al.*, "Enhanced electrochemical performance and storage mechanism of LiFePO₄ doped by Co, Mn and S elements for lithium-ion batteries," *Electrochim Acta*, vol. 388, p. 138592, Aug. 2021, doi: 10.1016/J.ELECTACTA.2021.138592.
- [45] K. Persson *et al.*, "Lithium Diffusion in Graphitic Carbon," *J Phys Chem Lett*, vol. 1, no. 8, pp. 1176–1180, Apr. 2010, doi: 10.1021/jz100188d.
- [46] Z. El Kacemi, Z. Mansouri, A. Benyoussef, A. El Kenz, M. Balli, and O. Mounkachi, "First principle calculations on pristine and Mn-doped iron fluorophosphates as sodium-ion battery cathode materials," *Comput Mater Sci*, vol. 206, p. 111292, 2022, doi: <https://doi.org/10.1016/j.commatsci.2022.111292>.
- [47] J. Deb, N. Seriani, and U. Sarkar, "Ultrahigh carrier mobility of penta-graphene: A first-principle study," *Physica E Low Dimens Syst Nanostruct*, vol. 127, p. 114507, 2021, doi: <https://doi.org/10.1016/j.physe.2020.114507>.

Graphical abstract

The first principles calculation indicates a significant enhancement of the conductivity and the Li-ion diffusion of penta-graphene nanoribbons under an external electric field.

